HardwareX 3 (2018) 146–159

Contents lists available at ScienceDirect

HardwareX

journal homepage: www.elsevier.com/locate/ohx

Hardware Article

Lake imaging and monitoring aerial drone

Jean-Luc Liardon, Lukas Hostettler, Ludovic Zulliger, Karl Kangur, Nawaaz S. Gujja Shaik, D.A. Barry*

Laboratoire de technologie écologique (ECOL), Institut d'ingénierie de l'environnement (IIE), Faculté de l'environnement naturel, architectural et construit (ENAC), Ecole polytechnique fédérale de Lausanne (EPFL), 1015 Lausanne, Switzerland

ARTICLE INFO

Keywords:
4G network
Mobile
Streaming
Telemetry
UAV
Imagery
Autonomous aircraft
LIMONAD
Infrared
RGB
Parachute
BVLOS
IR

ABSTRACT

We describe the development of a BVLOS (Beyond Visual Line-Of-Sight) model aircraft (UAV). The broad design requirements included (i) fuselage capable of accommodating an imaging package or other instrumentation, (ii) suitability for over-lake BVLOS authorization in Switzerland, (iii) capability of land or water take-offs/landing, (iv) at least 90-min flight autonomy, (v) modularity of the imaging package and (vi) real-time IR/RGB imagery. Requirement (i) was to ensure an aircraft amenable to future developments. Requirements (ii)–(iv) were driven by the goal of improving estimates of lake surface energy fluxes, since such fluxes have a major impact on long-term lake temperatures and hence ecological status. Requirement (v), in conjunction with (i), allows the UAV to be adapted to other imaging applications. The real-time imagery requirement (vi) permits modifications of on-going missions to map areas of specific interest as they are detected. The prototype UAV produced to satisfy these characteristics was built on the twin-motor My Twin Dream (MTD) aircraft, which has a 1.8-m wing span airframe and a spacious fuselage. The legal authorization necessitated, where feasible, hardware redundancy as well as installation of a parachute system. Continuous communication between the ground station and UAV is provided by the LTE cellular telephone network. The UAV communication is handled by an on-board Linux computer, which is also responsible for control of the imagery package. The avionics involved modifications of the open-source APM autopilot software and the associated ground control station. A key modification was to support a custom-built emergency recovery system, which is triggered by loss of a heart-beat signal from the autopilot. The MTD airframe was modified to accommodate the system electronics and imaging hardware. Results from test flights over Lake Geneva demonstrate the ability of the aircraft to produce imagery data.

1. Introduction

The use of unmanned aerial vehicles (UAVs) for environmental imaging is a rapidly developing field (e.g., [1–5]). One application domain of UAVs is quantification of energy fluxes from lakes, since such fluxes are essential for determining the rate of change of water temperature (e.g., [6–8]). These fluxes depend strongly on lake surface water temperature measurements (LSWT, e.g., [9–11]). Satellites are well established means for obtaining synoptic LSWT data (e.g., [12–14]), but at relatively coarse resolutions, e.g., about 100 m^2 for Landsat measurements [15]. Other factors limiting the usefulness of satellite thermal imagery are that it is occluded by cloud cover and is collected at different frequencies, e.g., once per 8 d for Landsat. Unsurprisingly, for certain applications such as

* Corresponding author.
E-mail address: andrew.barry@epfl.ch (D.A. Barry).

https://doi.org/10.1016/j.ohx.2017.10.003

Acronyms

3G/4G	Third/Fourth Generation mobile telecommunication technology
APM	AutoPilot Mega
BVLOS	Beyond Visual Line-Of-Sight
ESC	Electronic Speed Controller
FPV	First Person View
GPS	Global Positioning System
GSM	Global System for Mobile communication
HD	High Definition
ImPROV	Imaging Package for Remotely Operated Vehicle
IMU	Inertial Motion Unit
IR	InfraRed
ISP	In-System Programming
LED	Light-Emitting Diode
LIMONAD	Lake Imaging and MONitoring Aerial Drone
LTE	Long Term Evolution
LiPo	Lithium Polymer
LSWT	Lake Surface Water Temperature
LWIR	Long-Wave InfraRed
MTD	My Twin Dream
NMOS	N-type Metal–Oxide–Semiconductor
OSF	Open Science Framework
PPM	Pulse-Position Modulation
PWM	Pulse-Width Modulation
RC	Remote Control or Radio Control
RGB	Red-Green–Blue
RTL	Return-To-Launch
UART	Universal Asynchronous Receiver/Transmitter
UAV	Unmanned Aerial Vehicle
USB	Universal Serial Bus
VPN	Virtual Private Network

Table 1
Specifications.

Hardware name	Lake Imaging and Monitoring Aerial Drone (LIMONAD)
Subject area	Environmental, planetary and agricultural sciences
Hardware type	Imaging tools
Open Source License	GPL
Cost of Hardware	€2000 (without FLIR camera)
Source File Repository	https://osf.io/2jn9f/

thermal discharges [16], higher resolution at specified times is desirable for qualitative or quantitative assessments, or as boundary conditions in numerical models.

As part of on-going research on Lake Geneva, we are measuring LSWT using two platforms, a He-filled balloon that carries a custom-built package for LWIR (long-wave infrared) and RGB (red-green-blue) imagery [17], and a model aircraft. The balloon is limited in speed since it must be tethered to a boat and is subject to wind disturbances. However, it provides high-resolution images under light winds, although the overall spatial coverage that can be measured in a day is only a few square km at best. It is typically launched to heights of about 600–1000 m, and is set up to return LWIR images with pixel resolutions of about 1 m (at the deployment height of 600 m). Long transects, imaged rapidly such that the ambient atmospheric conditions are near-uniform, are not feasible with a balloon. In addition, balloon deployments are logistically demanding, which limits missions to relatively infrequent events. Therefore, a second aerial platform was developed to image LSWT more rapidly, and with reduced logistical support. The needs of this second platform are (Table 1):

BVLOS Suitable for authorization in Switzerland (specifically, Lake Geneva)
Water resistant Capability of both land and water take-offs/landings
Quick deployment Operational in less than 15 min
Real-time IR/RGB imagery Frequency sufficient to produce overlapped images for subsequent photogrammetry and analysis
Modular payload Modularity of the imaging package to easily change the setup and/or to transfer it to different vehicles
Autonomy More than 90 min flight autonomy
Configurability Spacious fuselage to enable different instrument/imaging packages for as-yet-unknown tasks

There is a substantial body of research covering all aspects of software and hardware pertaining to UAVs [18–28], with reviews of general aspects [29], domain-specific applications [30,31] and as imaging platforms [32]. Imaging UAVs are commonplace, with numerous innovative products appearing in recent years, along with downward pressure on prices. For example, the DJI Inspire + Zenmuse XT thermal camera[1] is a complete, off-the-shelf solution with a high quality thermal camera mounted on a gimbal, supported by a stable drone. On the other hand, the autonomy of this quadrotor is limited (about 20 min), and it cannot land on water. Fixed wing aircraft, such as the eBee Plus,[2] are also available. Like the just-mentioned DJI Inspire, this is a professional product, and has an autonomy of about 1 h. However, it is not suitable for water deployments, and does not provide real-time imagery. In addition, these UAVs are unable to capture IR and RGB imagery simultaneously, nor are they suitable for BVLOS

[1] http://www.dji.com/zenmuse-xt, last accessed 14 October 2017.
[2] https://www.sensefly.com/drones/ebee-plus.html, last accessed 14 October 2017.

deployments. Similarly, other UAVs are unable to satisfy the requirements listed above. LIMONAD (Lake Imaging and MONitoring Drone) was developed to achieve these goals.

LIMONAD is built on the My Twin Dream[3] (MTD) twin-motor model aircraft airframe. This 180-cm wingspan aircraft can support a total mass of 5.5 kg, allowing it to be configured for the autonomy and payload needed for missions of up 100 km or more. In short, the MTD was modified to accommodate different added components as follows (full details given in subsequent sections):

Water resistance Several adaptations were made to make the MTD water-resistant. Except for the top hatches (Fig. 11c), the fuselage was made watertight using fiberglass and epoxy coating. The downward-pointing imagers are installed in a 3D-printed housing and sealed with mastic. Top hatches, which must be opened frequently, are tightly inserted with neoprene gaskets. Waterproof servomotors were used, as these are exposed to direct splash in lake deployments.

Parachute landing system A parachute system was determined to be most suitable for over-water deployments. The main reasons for this choice were, (i) the additional weight is minimized, (ii) flying characteristics remain unchanged, (iii) the system is simple and reliable, and (iv) it is easily adapted to handle emergencies. The choice of parachute was made after a paper exercise where different solutions were evaluated. Besides the parachute option, this exercise led to field testing of a design based on the addition of floats to the MTD airframe. By comparison with the parachute solution, the floats increased the stall speed, reduced the autonomy, required smooth water for take-offs/landings, and in emergencies uncontrolled descents remained a significant risk.

Imaging/Communication Previously, we developed a versatile imaging package, called ImPROV [17]. This package is used in LIMONAD with a custom 3D-printed housing that carries thermal and RGB cameras. Importantly for BVLOS, ImPROV includes 4G/LTE communications, as such networks are both ubiquitous and reliable. This capability enables continuous, real-time encrypted communication between the ground station and UAV.

Autonomous flight The open-hardware Pixhawk[4] autopilot together with the open-source APM[5] stack makes missions fully autonomous. If desired, e.g., for BVLOS, missions can be geofenced both horizontally and vertically.

Autonomy On a single battery, LIMONAD can fly up to 100 min, with 15% power reserve remaining. The aircraft can also be flown with two 22 Ah batteries, with an autonomy of at least 180 min.

Emergencies The APM flight stack was modified to deal with different emergencies, with or without operator intervention. Depending on the situation, the aircraft can (i) circle and wait for instructions, (ii) return to launch or other location, or (iii) power down and launch the parachute. Note that in all failure situations, the aircraft has (iii) as the endpoint. This avoids, for instance, any possibility of this 5-kg aircraft flying uncontrolled at 55 km/h.

ImPROV payload As mentioned, the ImPROV package includes 4G/3G communication, real-time thermal and RGB Imagery, and is modular. The payload is switched off after parachute launch to protect the cameras in case of water leaks.

Ease-of-Use The airplane can be hand-launched from a small boat, perform autonomous, geofenced missions, land on water, provide real-time imagery and, if necessary, be manually controlled using a standard RC device.

2. LIMONAD design

This section provides an overview of the different development steps in LIMONAD. Build instructions are detailed in *Build_MTD.docx*, available on the OSF repository (Open Science Framework): https://osf.io/zrf6g/.

LIMONAD can be split into four parts:

Frame Body of the airplane including motors, servomotors, ESCs (Electronic Speed Controllers)
Autopiloting Autopilot (Pixhawk), sensors, RC (Remote Control)
Parachute System Parachute launcher with custom board
ImPROV Adapted, waterproof version of the ImPROV imaging package

Table 2 lists all the designed parts of the project.

2.1. Frame

The frame is based on the MTD[6] model aircraft, produced by My Fly Dream.[7] Our setup incorporates waterproof servomotors and,

[3] http://www.myflydream.com/, last accessed 14 October 2017.
[4] https://pixhawk.org/, last accessed 14 October 2017.
[5] http://ardupilot.org/, last accessed 14 October 2017.
[6] http://www.fpvmodel.com/mytwindream-1800mm-fpv-plane_g999.html, last accessed 14 October 2017.
[7] http://myflydream.com/, last accessed 14 October 2017.

Table 2
Design files.

Design file name	File type	License	File location
Frame			
Head	3D (STL)	GPL	https://osf.io/e6xuy/
HeadBase	3D (STL)	GPL	https://osf.io/qa6hm/
Servo-cover	3D (STL)	GPL	https://osf.io/xkyht/
Autopiloting			
SimpleBox	3D (STL)	GPL	https://osf.io/cj4wy/
ArduPlane-v2.px4	Firmware	GPL	https://osf.io/ab85u/
MTD.params	Parameters file	GPL	https://osf.io/ab85u/
Parachute system			
ParaAero	3D (STL)	GPL	https://osf.io/wgufz/
ParaBase	3D (STL)	GPL	https://osf.io/m7t64/
ParaBox	3D (STL)	GPL	https://osf.io/rndmu/
ParaCap	3D (STL)	GPL	https://osf.io/rehsw/
EmergencyRecoverV2	PCB (Eagle)	GPL	https://osf.io/h6apn/
EmergencySystem.ino	Firmware (Arduino)	GPL	https://osf.io/n2u9e/
ImPROV			
Lidv2	3D (STL)	GPL	https://osf.io/fytdj/
RasPi_holder	3D (STL)	GPL	https://osf.io/v28fa/
Scientific_rack	3D (STL)	GPL	https://osf.io/2xb7r/
Underside	3D (STL)	GPL	https://osf.io/bqxd8/
Wall	3D (STL)	GPL	https://osf.io/drz7q/
Webcam_holder	3D (STL)	GPL	https://osf.io/6afzu/
Relay Board	PCB (Eagle)	GPL	https://osf.io/qnkue/
Mtd_image.zip	Linux image	GPL	https://osf.io/vsdwx/

to facilitate easy hand-launching, motors that are more powerful than recommended. The airplane was waterproofed using layers of fiberglass and mastic. The nose was modified to make it more spacious and waterproof. For this purpose, a 3D-printed part was made for the top part of the nose, which carries a camera, a GPS receiver, and an airspeed sensor. The joints of the control surfaces were reinforced using plastic hinges.

2.1.1. Power configuration

The MotoCalc[8] tool was used to select the motor/propeller/battery combination, considering both hand launching and autonomy. The setup is presented in Table 3.

Fig. 1 displays a simulation of the performance with the chosen power setup. The configuration shows that at 60% throttle, the neutral lift airspeed is 16 m/s, with an autonomy of 2 h, giving a maximum mission distance of over 100 km with 10% battery reserve. Field testing confirmed that the design is close to achieving these criteria.

2.1.2. Waterproofing

The aircraft must be waterproof when floating, and able to resist water ingress into the fuselage during parachute landings. For the former requirement, the bottom half of the fuselage was fiberglassed with epoxy sealant, while for the latter, topside hatches were made water resistant using neoprene surrounds, as shown in Figs. 2 and 4.

Servomotors (for control surface movement) installed in the wings and tail are directly exposed to water splash, and so waterproof servomotors[9] were used. Mastic was used to glue and fill the gaps after installation of servomotors into the fuselage, resulting in a waterproof seal at these locations (Fig. 3).

2.1.3. Drone head

The aircraft has two hatches, one for the parachute near the center-of-gravity, and one in the nose for battery access. The latter requires special attention as the aircraft is slightly nose-heavy for aerodynamic stability. In addition, it is the preferred position for the airspeed sensor (Pitot tube) since this instrument should be exposed to undisturbed airflow. BVLOS missions require a redundant GPS sensor, which was also installed in the nose section. We designed a 3D-printed piece that fitted into the top of the aircraft's nose. This piece was made water-resistant with neoprene joints and mastic sealant. Fig. 4a shows the stock MTD head, while Fig. 4b and c show the base of the 3D-printed piece and the whole piece, respectively. An alternative nose section was designed, which in addition supported a front-pointing RGB camera, suitable for FPV missions (not shown here).

The head is designed so that the top half attaches to the bottom with three screws, which compresses the neoprene seal, making the head watertight. The airspeed sensor and the GPS receiver are placed on the top part to protect them from water. The bottom part

[8] http://www.motocalc.com, last accessed 14 October 2017.
[9] http://hitecrcd.com/products/servos/waterproof-servos-2/hs-5086wp-digital-waterproof-micro-servo/product, last accessed 14 October 2017.

Table 3
Power setup.

Motors	Scorpion SII-3014-1220KV
Propellers	APC Elektro Propeller 9 × 6E (P)
Battery	Maxamps LiPo 3S 22000 mAh

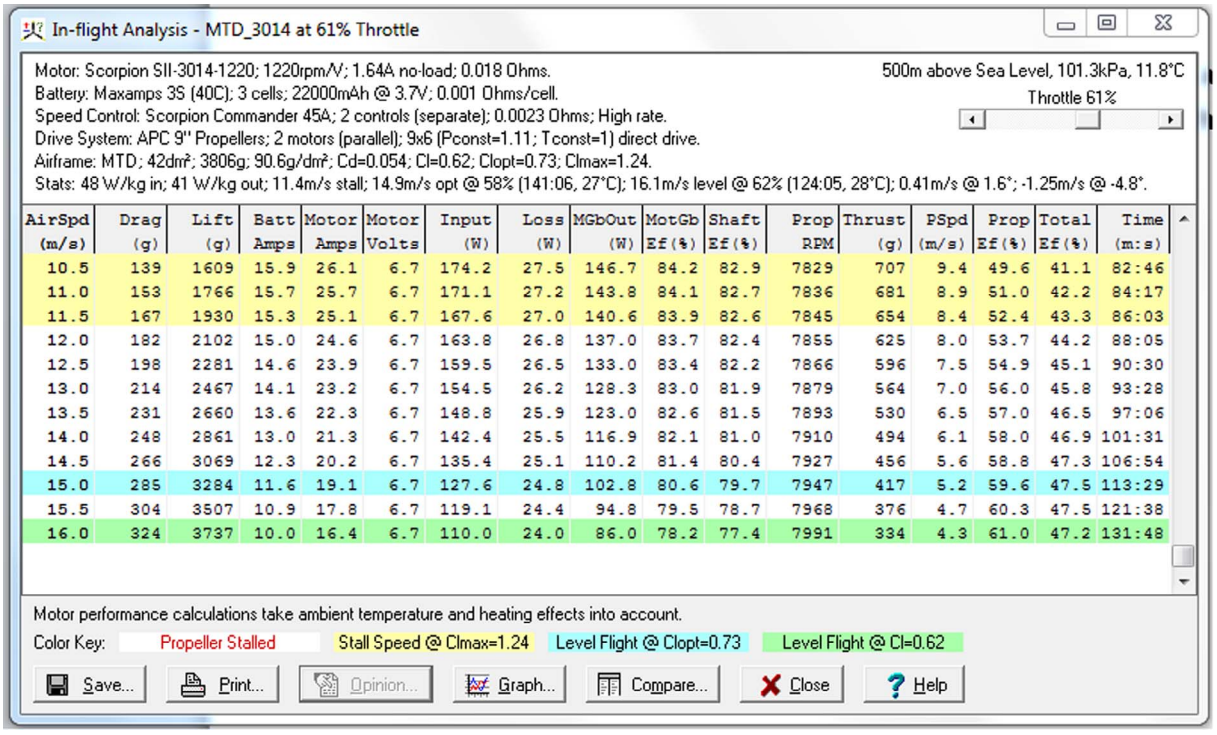

AirSpd (m/s)	Drag (g)	Lift (g)	Batt Amps	Motor Amps	Motor Volts	Input (W)	Loss (W)	MGbOut (W)	MotGb Ef(%)	Shaft Ef(%)	Prop RPM	Thrust (g)	PSpd (m/s)	Prop Ef(%)	Total Ef(%)	Time (m:s)
10.5	139	1609	15.9	26.1	6.7	174.2	27.5	146.7	84.2	82.9	7829	707	9.4	49.6	41.1	82:46
11.0	153	1766	15.7	25.7	6.7	171.1	27.2	143.8	84.1	82.7	7836	681	8.9	51.0	42.2	84:17
11.5	167	1930	15.3	25.1	6.7	167.6	27.0	140.6	83.9	82.6	7845	654	8.4	52.4	43.3	86:03
12.0	182	2102	15.0	24.6	6.7	163.8	26.8	137.0	83.7	82.4	7855	625	8.0	53.7	44.2	88:05
12.5	198	2281	14.6	23.9	6.7	159.5	26.5	133.0	83.4	82.2	7866	596	7.5	54.9	45.1	90:30
13.0	214	2467	14.1	23.2	6.7	154.5	26.2	128.3	83.0	81.9	7879	564	7.0	56.0	45.8	93:28
13.5	231	2660	13.6	22.3	6.7	148.8	25.9	123.0	82.6	81.5	7893	530	6.5	57.0	46.5	97:06
14.0	248	2861	13.0	21.3	6.7	142.4	25.5	116.9	82.1	81.0	7910	494	6.1	58.0	46.9	101:31
14.5	266	3069	12.3	20.2	6.7	135.4	25.1	110.2	81.4	80.4	7927	456	5.6	58.8	47.3	106:54
15.0	285	3284	11.6	19.1	6.7	127.6	24.8	102.8	80.6	79.7	7947	417	5.2	59.6	47.5	113:29
15.5	304	3507	10.9	17.8	6.7	119.1	24.4	94.8	79.5	78.7	7968	376	4.7	60.3	47.5	121:38
16.0	324	3737	10.0	16.4	6.7	110.0	24.0	86.0	78.2	77.4	7991	334	4.3	61.0	47.2	131:48

Fig. 1. Preparatory design of the LIMONAD power configuration.

fits into the fuselage, and allows installation of two batteries, each 22 Ah, inside the airplane. The bottom part is glued to the fuselage using mastic.

2.1.4. Joint reinforcement

As manufactured, the MTD control surfaces are fragile, and should be replaced with plastic hinges, as shown in Fig. 5.

2.2. Autopilot

Pixhawk is generally recognized as the best open-source autopilot on the market and was therefore used in LIMONAD. The APM flight stack was selected to be used with the Pixhawk as it is open source (with an extensive user base), easy to customize and, since it is widely used, reliable. Nevertheless, for the BVLOS solution, the APM was modified to add additional security and failsafe pathways.

The Pixhawk is built with partial dual redundancy with two Inertial Motion Units (IMUs) and two processors. Hardware redundancy was extended by including two GPS receivers. Aircraft safety was markedly increased by inclusion of a parachute system. The system design ensures that the parachute launches automatically in the event of autopilot failure or loss of power (e.g., battery failure). For this purpose, a heartbeat signal is sent from the autopilot to the parachute system: If the heartbeat is stopped the parachute will be launched (see Section 2.3 for more details).

2.2.1. Hardware

The autopilot uses in-built and external sensors to control the airplane efficiently. Table 4 shows the main sensors needed for this purpose. The Pitot tube is the only sensor without a like-for-like backup, however ground speed taken from the GPS tracking is used in case of failure. Fig. 6 shows the autopilot, GPS receiver model, and Pitot tube used.

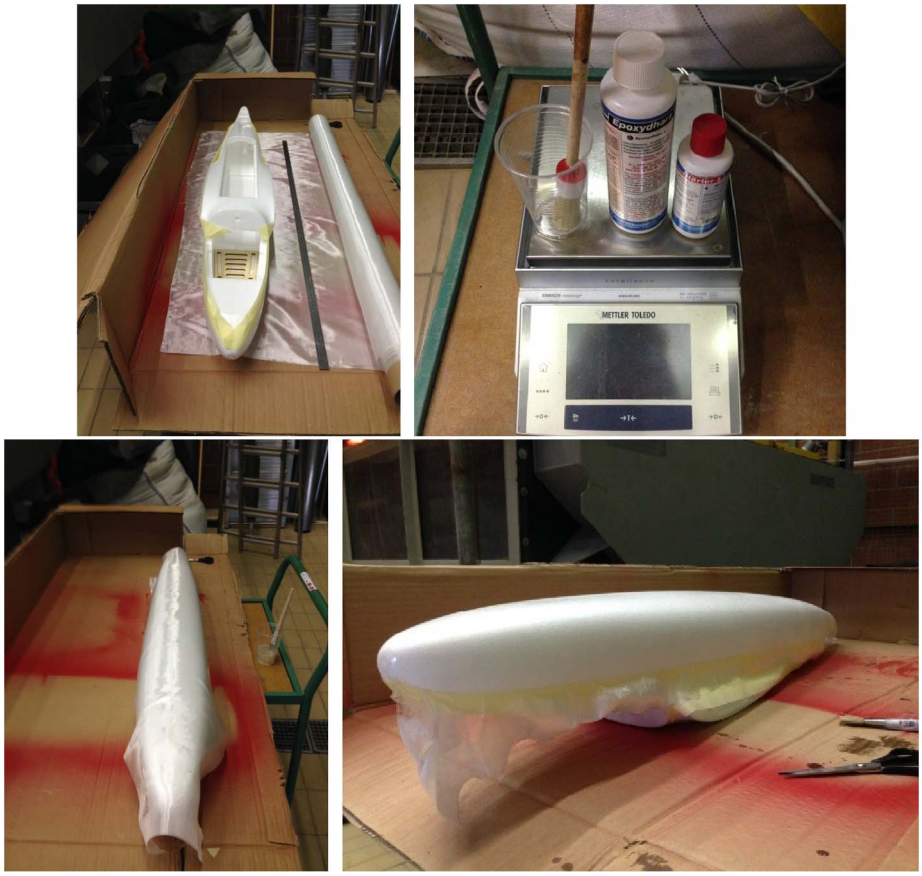

Fig. 2. Fiberglass is epoxied to the fuselage.

Fig. 3. Waterproof servomotors installed with mastic.

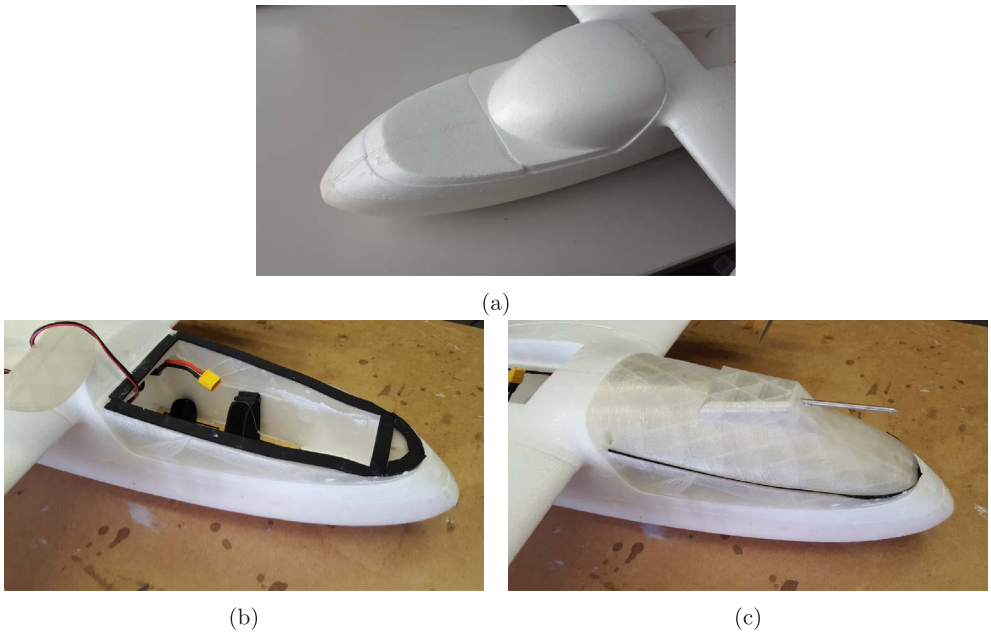

Fig. 4. (a) MTD head before modification, (b) base section of the 3D-printed nose section, showing the neoprene seal, and (c) completed 3D-printed nose section. Although not obvious in (c), the top section attaches to the bottom with three screws, which compress the neoprene seal.

Fig. 5. Elevator attached with (white) plastic hinges, which are glued into the frame and edge of the elevator surface.

Table 4
Essential sensors for autonomous operations of LIMONAD.

Data	Sensors	Location	Redundancy
Height	Barometer	Autopilot	Yes
Attitude	Gyroscope, Accelerometer, Magnetometer	Autopilot	Yes
Position	GPS receivers	Fuselage	Yes
Airspeed	Pitot tube	Fuselage	No

Fig. 6. Autopiloting hardware: Pixhawk autopilot, GPS receiver, Pitot tube.

Table 5
Failure pathway/reaction list.

Action number	Description
1	Ask operator for action I = Ignore, R = RTL, P = Parachute Default in **bold**
2	Return-to-launch (RTL)
3	Launch parachute
4	Heartbeat stopped. Launch parachute
Failure	**Reaction (Responses)**
Battery monitor unstable	1 (**I**,R)
Battery low	1 (I,**R**,P)
Battery critical	1 (R,**P**)
Battery dead	4
Barometer unhealthy	1 (I,**R**)
No GPS fix for 30 s	1 (I,**R**)
Barometer unhealthy & No GPS fix	1 (I,R,**P**)
Altitude > Pre-set limit for 10 s	1 (I,**R**)
Altitude > Pre-set limit for 60 s	1 (I,R,**P**)
Communication lost for 50 s	1 (I,**R**)
(Horizontal) Geofence breached	1 (I,**R**)
RC (radio control) lost while in manual mode	2
Autopilot failure	4
Uncontrolled descent/ mechanical failure	3

Fig. 7. Parachute launcher (left) and parachute (right).

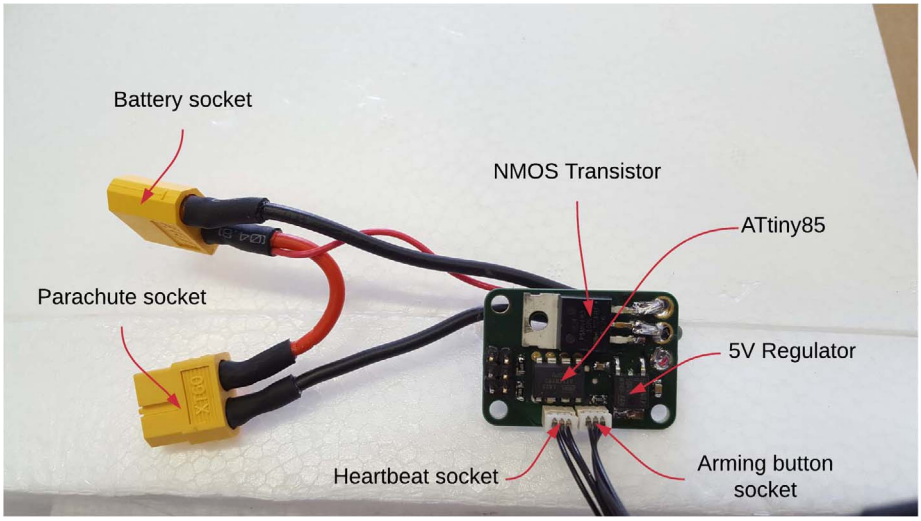

Fig. 8. Custom board for parachute launch control.

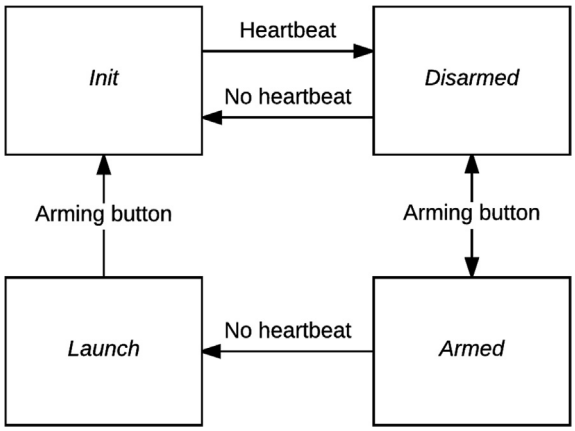

Fig. 9. Parachute launcher system state machine.

Fig. 10. LIMONAD imaging package comprising IR and RGB cameras, automated (position) or manual image control, real-time streaming and ground-station communication, housed in a watertight, 3D-printed box. Left: Package ready for installation into the airplane, showing removable USB storage and 4G communication dongle. Right: Interior of the package, which is described in detail by [17].

Table 6
Operational characteristics of the LIMONAD UAV configured for imaging missions.

Weight	5 kg
Speed	45 to 100 km/h, cruise at 55 km/h
Maximum operational wind speed (as tested)	Up to 50 km/h
Autonomy	100 min

2.2.2. Software

As mentioned, we customized the APM flight stack, which can be downloaded from Ardupilot Github.[10] Our modified flight stack is based on ArduPlane 3.5.3. Table 5 summarizes the implemented extra failure-reaction behaviors.

Another modification to the APM stack was the implementation of a robust parachute communication system with the following features:

Heartbeat A square 20 ms heartbeat signal is generated by the autopilot. Stopping the heartbeat launches the parachute.
Arming state The parachute system provides its arming state to the autopilot. The airplane cannot be armed without first arming the parachute system.
Stop motors When the heartbeat is stopped so do the motors. There is a failsafe to reactivate the motors in case of a parachute launch failure.

2.3. Parachute system

The parachute system should fulfil the following needs:

Light and compact Important to minimize weight.
Low impact shock Parachute cannot be too small.
Reliability The launching technology must be reliable.

[10] https://github.com/ArduPilot/ardupilot, last accessed 14 October 2017.

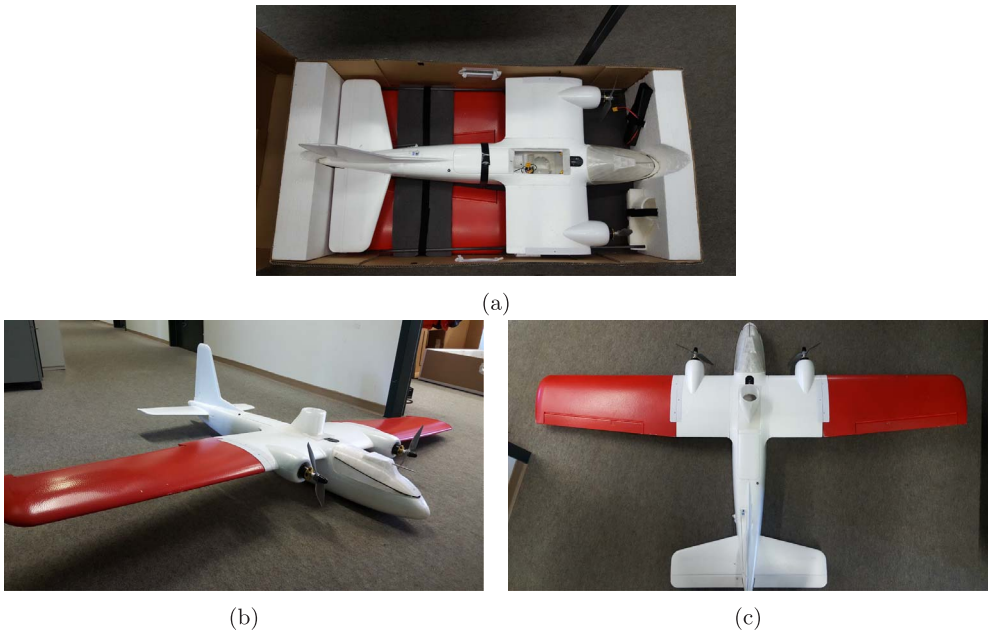

Fig. 11. (a) LIMONAD packed inside its box for transport, (b) assembled, and (c) top view.

Failsafe In case of autopilot or battery failure, which are emergency conditions, the parachute must launch.

There are many different parachute launchers available. Launch technologies utilize compressed carbon dioxide, servomotors, springs, fuses, etc. We selected a lightweight launcher based on a simple fuse trigger and a spring mechanism. Fig. 7 shows the chosen parachute launcher, from Skycat,[11] and parachute, from Fruity Chutes.[12]

Triggering the parachute system is key to ensuring the safety of the aircraft as an autonomous vehicle. For this purpose, a heartbeat signal is generated by the autopilot. The heartbeat is a pre-defined, square pulse, which is received by a custom board, with an independent power supply, for triggering the parachute system. When the heartbeat stops or its frequency shifts, the board sends a current that burns the parachute launcher fuse and thereby initiates the parachute. This is a robust design since it handles any untoward failures including dead battery, autopilot hardware failure, or software hangs. In addition, for the different failure modes listed in Table 3, or for normal landings, the autopilot simply stops the heartbeat.

The custom parachute board has the following main components:

ATtiny85 Programmable microcontroller
NMOS transistor Enable or disable current in the parachute fuse
5V Regulator Power the microcontroller
Heartbeat socket Connection to the autopilot. An output line shares the arming state, and an input line gives the heartbeat
Arming button socket The LED displays state to the user and button toggles the arming of the parachute
Battery socket Simple connector to the dedicated battery
Parachute fuse socket Connection to the parachute fuse

Fig. 8 displays the board and its different components.

The ATtiny85 microcontroller controls the NMOS transistor, the LED arming button, and communicates with the autopilot. It can be programmed using an ISP Programmer such as the Arduino ISP.[13] Arduino software is used to build and flash the program. The system logic is organized into four states: *Init*, *Disarmed*, *Armed* and *Launch*. *Init* is the first state, when there is no heartbeat, and the system is disarmed. When the heartbeat is successfully detected the state becomes *Disarmed*. If the arming button is pressed for about 2 s, the state becomes *Armed*. In this state, the button LED is ON, and the system will go to the *Launch* state if heartbeat is lost. In the *Launch* state, the NMOS transistor is switched ON for about 2 s (enough to burn the parachute fuse) and the button LED blinks until it is pressed, which resets the system to the *Init* state. Fig. 9 displays the state machine.

[11] https://www.skycat.pro/shop/parachutes, last accessed 14 October 2017.
[12] https://fruitychutes.com/, last accessed 14 October 2017.
[13] https://www.arduino.cc/en/Main/ArduinoISP, last accessed 14 October 2017.

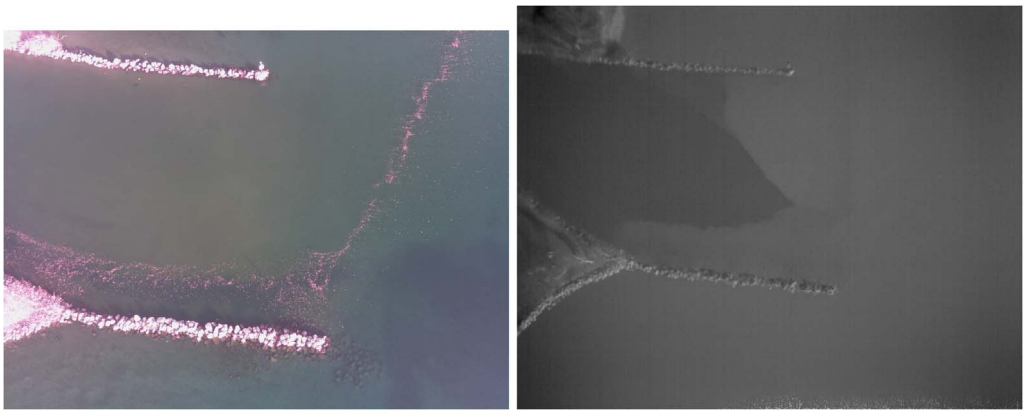

(a) Discharge of the Venoge River into Lake Geneva. The left (RGB) image shows the river entering the lake. The lakebed is distinguishable due to the shallow water depth. The right IR (which senses only the water surface) image shows the disappearance of the river discharge due to negative buoyancy of the inflow. Images taken from a 70 m height, with an aircraft speed of 45 km/h.

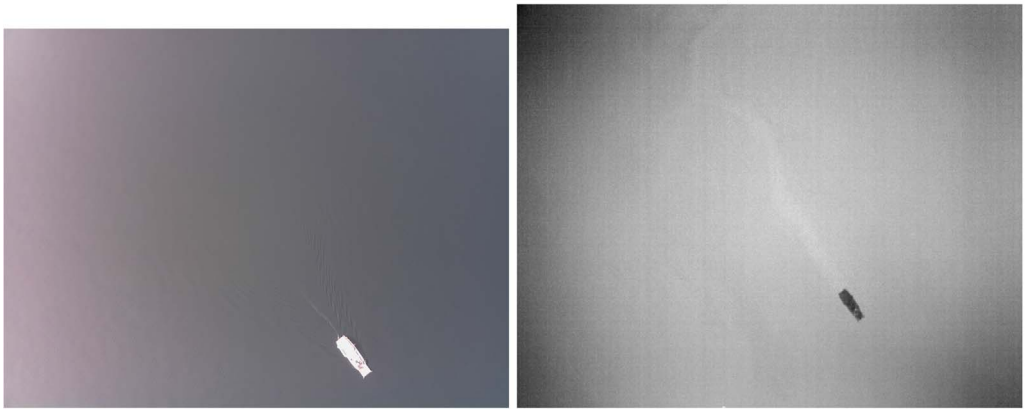

(b) Sailing boat (from which the airplane was hand-launched). Not much detail is seen in the RGB (left) image, whereas in the thermal (right) image, the path of the boat is clear in the trail when surface water is displaced by below-surface water (the surface and below surface water temperatures are different). In this somewhat unusual case, the surface water is colder than the below-surface water, a situation that occurs when the air temperature drops abruptly.

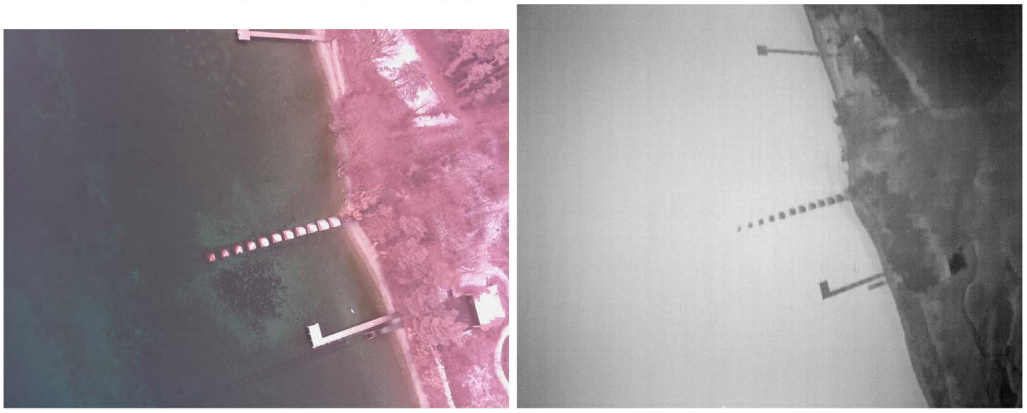

(c) A near-shore area of Lake Geneva, showing both land and lake. Here, the temperature of the water is higher than the land partly due to cold weather.

Fig. 12. LIMONAD payload image examples taken from missions over Lake Geneva, Switzerland.

2.4. ImPROV

Presently, the scientific payload features are:

- Thermal and RGB imagery, including live streaming
- FPV camera (optional)
- Communication over 3G/4G
- Waterproof
- Failsafe power relay

These features were fulfilled by adapting the ImPROV system, described in detail elsewhere [17]. The main modifications were:

Waterproof box A 3D-printed box that can be sealed using neoprene and screws.
Power relay A small custom board is used to allow the system to cut power. This protects the imaging package from accidental water leaks.
FPV Camera Optional FPV camera placed in the head of the airplane, as described in Section 2.1.3.
USB Hub Powers all the USB devices. Additional USB connections are available on the Raspberry Pi microcomputer (part of the standard ImPROV system).
FLIR Framegrabber Here, an alternative (with similar functionality) to that described by [17] is used.

A detailed description of the building steps is provided in *Build_MTD.docx*, which can be downloaded from this OSF repository. Fig. 10 shows the finished LIMONAD imaging package.

3. Performance

The performance of the LIMONAD UAV can be divided into two parts:

Plane The different observed properties of the airplane itself
Payload Some examples of acquired data collected during different missions

3.1. Plane

The final weight of the modified MTD is 5 kg. As envisaged in the original design, its powerful twin motors facilitate straightforward hand-launching, even from small boats. With the fuselage below the wings, the drone is stable in the air and not easily disturbed by wind. It has been tested in high wind speed conditions (50 km/h), during which it maintained sufficient stability to complete the mission and provide data. The LIMONAD autonomy is 100 min in good conditions, while maintaining a battery reserve of 15%. It is therefore suitable for long-duration, out-of-sight missions. Table 6 summarizes LIMONAD's operational characteristics. Using a handmade box the plane is safely transported to/from the field. Fig. 11 shows the packed and assembled LIMONAD.

3.2. Payload

The performance of the payload is described in [17]. Fig. 12 shows an example of the data obtained with LIMONAD. Note that the RGB images are taken with the camera's near infrared filter removed.

4. Conclusion

We developed a waterproof drone that can carry a fully customizable imaging package. The UAV can be built using off-the-shelf components, along with some custom 3D-printed parts and PCBs. The aircraft build included fiberglassing of the lower half of the fuselage. There are at present no other hand-launched UAVs that include a configurable and adaptable imaging package, live streaming from all on-board cameras and sensors, waterproof landings, BVLOS potential and autonomous flight. Of these features, we point out that no other existing BVLOS-ready drone can be hand-launched from a small boat and land on water. Importantly, without the payload, the LIMONAD UAV is inexpensive. The payload cost depends on the selected hardware, and would in most cases be the most costly part of the vehicle.

The LIMONAD performance makes it valuable for on-water missions, where launching and retrieval are major issues. It features excellent usability (hand-launch, easy landing), security (redundancy, parachute system), and autonomy (more than 100 min with one battery). The reliability and ease-of-use of this platform has been assessed during numerous missions carried out over Lake Geneva. Full build instructions are available at this OSF repository.

Acknowledgements

The development of LIMONAD benefited from numerous persons working on different research and engineering projects related to our research on Lake Geneva. We offer our thanks to Beat Geissmann, Samuel Benketaf, Philippe Paccaud, Ulrich Lemmin, and Abolfazl Irani Rahaghi. Partial financial support was provided by SNF 159422.

References

[1] R.A. de Oliveira, A.M.G. Tommaselli, E. Honkavaara, Using hyperspectral frame images from unmanned airborne vehicle for detailed measurement of boreal forest 3D structure, IOP Conf. Ser.: Earth Environ. Sci. 44 (4) (2016) 042029, http://dx.doi.org/10.1088/1755-1315/44/4/042029.
[2] E. Honkavaara, M.A. Eskelinen, I. Pölönen, H. Saari, H. Ojanen, R. Mannila, C. Holmlund, T. Hakala, P. Litkey, T. Rosnell, N. Viljanen, M. Pulkkanen, Remote sensing of 3-D geometry and surface moisture of a peat production area using hyperspectral frame cameras in visible to short-wave infrared spectral ranges onboard a small unmanned airborne vehicle (UAV), IEEE Trans. Geosci. Remote Sens. 54 (9) (2016) 5440–5454, http://dx.doi.org/10.1109/TGRS.2016.2565471.
[3] E.F. Berra, R. Gaulton, S. Barr, Use of a digital camera onboard a UAV to monitor spring phenology at individual tree level, in: IEEE International Geoscience and Remote Sensing Symposium (IGARSS), 2016, pp. 3496–3499, http://dx.doi.org/10.1109/IGARSS.2016.7729904.
[4] J. Suomalainen, N. Anders, J. Franke, H. Bartholomeus, C. Nolet, M. van Puijenbroek, H. Kramer, S. Keesstra, S. Mücher, L. Kooistra, Overview of UAV activities in Wageningen unmanned aerial remote sensing facility, ISPRS – International Archives of the Photogrammetry, Remote Sensing and Spatial Information Sciences XL-1/W4 (2015) 261–262, http://dx.doi.org/10.5194/isprsarchives-XL-1-W4-261-2015.
[5] J. Suomalainen, N. Anders, J. Franke, H. Bartholomeus, C. Nolet, M. van Puijenbroek, H. Kramer, S. Keesstra, S. Mücher, L. Kooistra, Overview of UAV activities in Wageningen unmanned aerial remote sensing facility, ISPRS – International Archives of the Photogrammetry, Remote Sensing and Spatial Information Sciences XL-1/W4 (2015) 261–262, http://dx.doi.org/10.5194/isprs-archives-XLI-B8-953-2016.
[6] R. McGloin, H. McGowan, D. McJannet, F. Cook, A. Sogachev, S. Burn, Quantification of surface energy fluxes from a small water body using scintillometry and eddy covariance, Water Resour. Res. 50 (1) (2014) 494–513, http://dx.doi.org/10.1002/2013WR013899.
[7] M.R. Magee, C.H. Wu, Effects of changing climate on ice cover in three morphometrically different lakes, Hydrol. Process. 31 (2) (2017) 308–323, http://dx.doi.org/10.1002/hyp.10996.
[8] B.M. Kraemer, O. Anneville, S. Chandra, M. Dix, E. Kuusisto, D.M. Livingstone, A. Rimmer, S.G. Schladow, E. Silow, L.M. Sitoki, R. Tamatamah, Y. Vadeboncoeur, P.B. McIntyre, Morphometry and average temperature affect lake stratification responses to climate change, Geophys. Res. Lett. 42 (12) (2015) 4981–4988, http://dx.doi.org/10.1002/2015GL064097.
[9] B.M. Lofgren, Y. Zhu, Surface energy fluxes on the Great Lakes based on satellite-observed surface temperatures 1992 to 1995, J. Great Lakes Res. 26 (3) (2000) 305–314, http://dx.doi.org/10.1016/S0380-1330(00)70694-0.
[10] S. Moukomla, P.D. Blanken, Remote sensing of the North American Laurentian Great Lakes' surface temperature, Remote Sens. 8 (4) (2016) 286, http://dx.doi.org/10.3390/rs8040286.
[11] R.I. Woolway, I.D. Jones, D.P. Hamilton, S.C. Maberly, K. Muraoka, J.S. Read, R.L. Smyth, L.A. Winslow, Automated calculation of surface energy fluxes with high-frequency lake buoy data, Environ. Model. Softw. 70 (2015) 191–198, http://dx.doi.org/10.1016/j.envsoft.2015.04.013.
[12] C. Wloczyk, R. Richter, E. Borg, W. Neubert, Sea and lake surface temperature retrieval from Landsat thermal data in Northern Germany, Int. J. Remote Sens. 27 (12) (2006) 2489–2502, http://dx.doi.org/10.1080/01431160500300206.
[13] S. Pareeth, N. Salmaso, R. Adrian, M. Neteler, Homogenised daily lake surface water temperature data generated from multiple satellite sensors: a long-term case study of a large sub-Alpine lake, Sci. Rep. 6 (2016) 31251, http://dx.doi.org/10.1038/srep31251.
[14] S. Pareeth, M. Bresciani, F. Buzzi, B. Leoni, F. Lepori, A. Ludovisi, G. Morabito, R. Adrian, M. Neteler, N. Salmaso, Warming trends of perialpine lakes from homogenised time series of historical satellite and in-situ data, Sci. Total Environ. 578 (2017) 417–426, http://dx.doi.org/10.1016/j.scitotenv.2016.10.199.
[15] D.P. Roy, M.A. Wulder, T.R. Loveland, C.E. Woodcock, R.G. Allen, M.C. Anderson, D. Helder, J.R. Irons, D.M. Johnson, R. Kennedy, T.A. Scambos, C.B. Schaaf, J.R. Schott, Y. Sheng, E.F. Vermote, A.S. Belward, R. Bindschadler, W.B. Cohen, F. Gao, J.D. Hipple, P. Hostert, J. Huntington, C.O. Justice, A. Kilic, V. Kovalskyy, Z.P. Lee, L. Lymburner, J.G. Masek, J. McCorkel, Y. Shuai, R. Trezza, J. Vogelmann, R.H. Wynne, Z. Zhu, Landsat-8: Science and product vision for terrestrial global change research, Remote Sens. Environ. 145 (2014) 154–172, http://dx.doi.org/10.1016/j.rse.2014.02.001.
[16] USEPA, Remote Sensing Report, Lake Ontario: Study of Thermal Discharges from Ginna Nuclear Power Station, Oswego Steam Power Station, and Nine Mile Point Nuclear Power Station, National Field Investigations Center, Denver, Colorado, 1975.
[17] J.-L. Liardon, D.A. Barry, Adaptable imaging package for remote vehicles, HardwareX 2 (2017) 1–12, http://dx.doi.org/10.1016/j.ohx.2017.04.001.
[18] C.J. Hall, D. Morgan, A. Jensen, H. Chao, C. Coopmans, M. Humpherys, Y. Chen, Team OSAM-UAV's design for the 2008 AUVSI student UAS competition, in: Proceedings of the ASME International Design Engineering Technical Conferences and Computers and Information in Engineering Conference 2009, DETC2009, vol. 3, 2010, pp. 575–584, doi:110.1115/DETC2009-86500.
[19] M. Leonardo, A. Jensen, Y. Chen, M. McKee, C. Coopmans, Fish track UAV payload system: A wildlife telemetry using UAV's for moving target and moving detector, in: Proceedings of the ASME 2013 International Design Engineering Technical Conference and Computers and Information in Engineering Conference (DETC2013, August 4–7, Portland, Oregon, USA, ASME/IEEE MESA, ASME IDETC/CIE), DETC2013-13444, 2013.
[20] A. Demario, P. Lopez, E. Plewka, R. Wix, H. Xia, E. Zamora, D. Gessler, A.P. Yalin, Water plume temperature measurements by an unmanned aerial system (UAS), Sensors (Switzerland) 17 (2) (2017), http://dx.doi.org/10.3390/s17020306.
[21] J. Bendig, A. Bolten, G. Bareth, Introducing a low-cost mini-UAV for thermal- and multispectral-imaging, International Archives of the Photogrammetry, Remote Sensing and Spatial Information Sciences – ISPRS Archives 39 (2012) 345–349, http://dx.doi.org/10.5194/isprsarchives-XXXIX-B1-345-2012.
[22] F. Andert, F.-M. Adolf, L. Goormann, J. Dittrich, Autonomous vision-based helicopter flights through obstacle gates, J. Intell. Rob. Syst.: Theory Appl. 57 (1–4) (2010) 259–280, http://dx.doi.org/10.1007/s10846-009-9357-3.
[23] M. Aljehani, M. Inoue, Communication and autonomous control of multi-UAV system in disaster response tasks, Smart Innov., Syst. Technol. 74 (2018) 123–132, http://dx.doi.org/10.1007/978-3-319-59394-4_12.
[24] Z. Fan, B. Guo, J. Hou, Implementation of a drone-based video streamer, Smart Innov., Syst. Technol. 82 (2018) 67–74, http://dx.doi.org/10.1007/978-3-319-63859-1_9.
[25] S. Bang, H. Kim, H. Kim, UAV-based automatic generation of high-resolution panorama at a construction site with a focus on preprocessing for image stitching, Autom. Constr. 84 (Supplement C) (2017) 70–80, http://dx.doi.org/10.1016/j.autcon.2017.08.031.
[26] P. Oettershagen, A. Melzer, T. Mantel, K. Rudin, T. Stastny, B. Wawrzacz, T. Hinzmann, S. Leutenegger, K. Alexis, R. Siegwart, Design of small hand-launched solar-powered UAVs: from concept study to a multi-day world endurance record flight, J. Field Rob. 34 (7) (2017) 1352–1377, http://dx.doi.org/10.1002/rob.21717.
[27] J. Wang, C. Jiang, Z. Han, Y. Ren, R. Maunder, L. Hanzo, Taking drones to the next level: cooperative distributed unmanned-aerial-vehicular networks for small and mini drones, IEEE Veh. Technol. Mag. 12 (3) (2017) 73–82, http://dx.doi.org/10.1109/MVT.2016.2645481.
[28] H. Huang, J. Long, H. Lin, L. Zhang, W. Yi, B. Lei, Unmanned aerial vehicle based remote sensing method for monitoring a steep mountainous slope in the Three Gorges Reservoir, China, Earth Sci. Inf. 10 (3) (2017) 287–301, http://dx.doi.org/10.1007/s12145-017-0291-9.

[29] S.G. Gupta, M. Ghonge, P. Jawandhiya, Review of unmanned aircraft system (UAS), Int. J. Adv. Res. Comput. Eng. Technol. 2 (4) (2013) 1646–1658.
[30] L. Pádua, J. Vanko, J. Hruška, T. Adão, J.J. Sousa, E. Peres, R. Morais, UAS, sensors, and data processing in agroforestry: a review towards practical applications, Int. J. Remote Sens. 38 (8–10) (2017) 2349–2391, http://dx.doi.org/10.1080/01431161.2017.1297548.
[31] J. Awange, Unmanned Aircraft Vehicles, Springer, International Publishing, Cham Switzerland, 2018 Ch. 20, pp. 423-443, http://dx.doi.org/10.1007/978-3-319-58418-820.
[32] F. Nex, F. Remondino, UAV for 3D mapping applications: a review, Appl. Geomatics 6 (1) (2014) 1–15, http://dx.doi.org/10.1007/s12518-013-0120-x.